Reduced and Excited States of (bpym)[PtCl 2] n (bpym = 2,2‘-Bipyrimidine; n = 1, 2): Experiments and DFT Calculations

ARTICLE *in* INORGANIC CHEMISTRY · SEPTEMBER 2002

Impact Factor: 4.76 · DOI: 10.1021/ic020158f · Source: PubMed

11 AUTHORS, INCLUDING:

Axel Klein
University of Cologne
185 PUBLICATIONS **2,897** CITATIONS
SEE PROFILE

Ioannis Tiritiris
Hochschule Aalen
80 PUBLICATIONS **269** CITATIONS
SEE PROFILE

Inorg. Chem. **2002**, *41*, 4139–4148

Reduced and Excited States of (bpym)[$PtCl_2$]$_n$ (bpym = 2,2′-Bipyrimidine; n = 1, 2): Experiments and DFT Calculations

Wolfgang Kaim,*,† Akbey Dogan,† Matthias Wanner,† Axel Klein,† Ioannis Tiritiris,† Thomas Schleid,† Derk J. Stufkens,‡ Theo L. Snoeck,‡ Eric J. L. McInnes,§ Jan Fiedler,|| and Stanislav Záliš||

Institut für Anorganische Chemie, Universität Stuttgart, Pfaffenwaldring 55, D-70550 Stuttgart, Germany, Institute of Molecular Chemistry, Universiteit van Amsterdam, Nieuwe Achtergracht 166, 1018 WV Amsterdam, The Netherlands, Department of Chemistry, The University of Manchester, Manchester M13 9PL, U.K., and J. Heyrovský Institute of Physical Chemistry, Academy of Sciences of the Czech Republic, Dolejškova 3, CZ-18223 Prague, Czech Republic

Received February 27, 2002

The complexes (bpym)$PtCl_2$ (**1**) and the new (μ-bpym)[$PtCl_2$]$_2$ (**2**), bpym = 2,2′-bipyrimidine, were synthesized and, in the case of **1**, crystallized in solvent-free form for X-ray diffraction. The molecules **1** exhibit two different kinds of stacking motifs in the crystal with an interstack CH--N interaction. Complexes **1** and **2** were found to be sufficiently soluble for cyclic voltammetry, spectroscopy (absorption and emission), and spectroelectrochemical studies (UV–vis, EPR). As a result of single or double coordination of the strongly σ-accepting [$PtCl_2$] fragment to bpym, the paramagnetic anions **1**$^{\bullet-}$ and **2**$^{\bullet-}$ and the dianions **1**$^{2-}$ and **2**$^{2-}$ could be reversibly generated, despite the presence of metal–halide bonds. DFT calculations of $A(^{195}Pt)$ and **g** tensor components confirm that the singly occupied MOs of the monoanionic species have mainly $\pi*$(bpym) character with nonnegligible platinum d orbital participation. The assignments of the electronic absorption and emission and resonance Raman spectra for both complexes are supported by DFT calculations.

Introduction

Although dichloroplatinum(II) complexes of α-diimine ligands such as 2,2′-bipyridine (bpy) or 2,2′-bipyrimidine (bpym) have been known now for some time,[1,2] these and related compounds have received increasing attention recently because of various special features:

(i) The complex photophysical behavior[3] of such materials such as variable temperature emission in the solid state or in solution is related to their ability to form aggregates (via stacking) between the largely planar molecules.[4,5] Differences in crystallization are also responsible for distinctly different color forms of e.g. yellow and red (bpy)$PtCl_2$.[5]

(ii) Chemical or electrochemical reduction produces paramagnetic complexes which are better formulated as Pt^{II}/radical anion compounds and not as Pt^{I} species.[6,7] EPR and spectroelectrochemical techniques were employed to characterize such one-electron reduced systems.[6,7]

(iii) Chloroplatinum compounds with ancillary nitrogen ligands are generally interesting for their physiological

* To whom correspondence should be addressed. E-mail: kaim@iac.uni-stuttgart.de.
† Institut für Anorganische Chemie.
‡ Institute of Molecular Chemistry.
§ The University of Manchester.
|| J. Heyrovsky Institute.

(1) Osborn, R. J.; Rogers D. *J. Chem. Soc., Dalton Trans.* **1974**, 1002.
(2) Kiernan, P. M.; Ludi, A. *J. Chem. Soc., Dalton Trans.* **1978**, 1127.
(3) (a) Connick, W. B.; Miskowski, V. M.; Houlding, V. H.; Gray, H. B. *Inorg. Chem.* **2000**, *39*, 2585 and literature cited. (b) Dungey, K. E.; Thompson, B. D.; Kane-Maguire, N. A. P.; Wright, L. L. *Inorg. Chem.* **2000**, *39*, 5192.
(4) Connick, W. B.; Marsh, R. E.; Schaefer, W. P.; Gray, H. B. *Inorg. Chem.* **1997**, *36*, 913.
(5) (a) Textor, V. M.; Oswald, H. R. *Z. Anorg. Allg. Chem.* **1974**, *407*, 244. (b) Herber, R. H.; Croft, M.; Coyer, M. J.; Bilash, B.; Sahiner, A. *Inorg. Chem.* **1994**, *33*, 2422. (c) Connick, W. B.; Henling L. M.; Marsh, R. E.; Gray, H. B. *Inorg. Chem.* **1996**, *35*, 6261.
(6) (a) MacGregor, S. A.; McInnes, E.; Sorbie, R. J.; Yellowlees, L. J. In *Molecular Electrochemistry of Inorganic, Bioinorganic and Organometallic Compounds*; Pombeiro, A. J. L., McCleverty, J. A., Eds.; Kluwer Academic Publishers: Dordrecht, The Netherlands, 1993; p 503. (b) Collison, D.; McInnes, E. J. L.; Mabbs, F. E.; Taylor, K. J.; Welch, A. J.; Yellowlees, L. J. *J. Chem. Soc., Dalton Trans.* **1996**, 329. (c) McInnes, E. J. L.; Farley, R. D.; Macgregor, S. A.; Taylor, K. J.; Yellowlees, L. J.; Rowlands, C. C. *J. Chem. Soc., Faraday Trans.* **1998**, *94*, 2985. (d) McInnes, E. J. L.; Farley, R. D.; Rowlands, C. C.; Welch, A. J.; Rovatti, L.; Yellowlees, L. J. *J. Chem. Soc., Dalton Trans.* **1999**, 4203. (e) Cf. also a study on [(terpy)PtCl]$^{\bullet}$: Hill, M. G.; Bailey, J. A.; Mishowski, V. M.; Gray, H. B. *Inorg. Chem.* **1996**, *35*, 4585.
(7) For organometallic analogues, see: (a) Vogler, C.; Schwederski, B.; Klein, A.; Kaim, W. *J. Organomet. Chem.* **1992**, *436*, 367. (b) Braterman, P. S.; Song, J.-I.; Wimmer, F. M.; Wimmer, S.; Kaim, W.; Klein, A.; Peacock, R. D. *Inorg. Chem.* **1992**, *31*, 5084. (c) Kaim, W.; Klein, A. *Organometallics* **1995**, *14*, 1176.

10.1021/ic020158f CCC: $22.00
Published on Web 07/12/2002

behavior inside cells and toward the DNA in continuing efforts for the advancement of metal-based tumor therapy.[8,9]

(iv) Platinum(II) compounds have a potential as catalysts and catalyst precursors for C−H bond activation.[10,11] It was reported that (bpym)$PtCl_2$ (**1**), bpym = 2,2′-bipyrimidine, is a robust catalyst precursor for efficient methane oxidation to methanol.[11a]

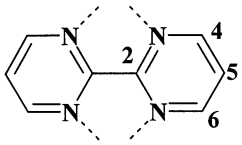

2,2-bipyrimidine = bpym

Whereas **1** has been studied since 1978[2] and two crystal structure analyses of solvated (bpym)$PtCl_2$ have appeared more recently,[4,12] it was reported that the obvious extension, the dinuclear compound (μ-bpym)$[PtCl_2]_2$, could not be obtained.[2] To our knowledge, there has not yet been any report of solution properties of a bis(dichloroplatinum(II)) complex with a π-conjugated bridging ligand. Drawing on previous experience with organometallic analogues (μ-bpym)$[PtR_n]_2$ (R = Me, n = 2, 4;[13,14] R = Mes,[13] *p*-Tol, Ad[15] n = 2), we have now succeeded in preparing (μ-bpym)-$[PtCl_2]_2$ (**2**). This report contains information on the reduced and excited states of **1** and **2**, based on electrochemical, EPR, UV−vis−spectroelectrochemical, emission, and resonance Raman (rR) studies. In addition, solvent-free **1** could be crystallized for structure analysis; the structural and spectroscopic data were interpreted using results from DFT calculations.

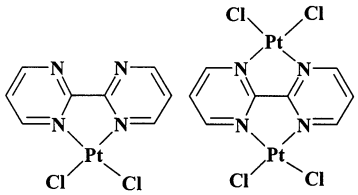

1 **2**

Further reasons for synthesizing dinuclear **2** and for studying its electrochemical and spectroscopic properties include a comparison with other dinuclear compounds of bridging bpym with complex fragments containing a platinum metal halide function such as (η^6-C_6R_6)$ClOs^{+16}$ or (η^5-C_5R_5)ClM^+ (M = Ir, Rh).[17] A related 5d metal halide fragment is $(OC)_3ClRe$, which has also been studied in bpym-bridged dinuclear form.[18] Additionally, the combination between the conjugated bridging ligand bpym with its relatively high-lying π* MO[19] and two electron-poor d^8 metal complex fragments [$PtCl_2$] was expected to produce on reduction a singly occupied MO of rather mixed metal/ligand character. For a symmetrical dinuclear compound a mixed-valent[13,20,21] (d^8/d^9) formulation could thus contribute to the description of the paramagnetic state as evident from EPR[22] or spectroelectrochemical studies.[23] Finally, the electronic structures of related bpym-bridged dinuclear compounds such as (μ-bpym)$[M(CO)_4]_2$[19] (M = Mo^0, W^0; d^6 configuration) have been studied by resonance Raman and emission spectroscopy.[24]

Experimental Section

Instrumentation. EPR spectra were recorded in the X band on a Bruker System ESP 300 equipped with a Bruker ER035M gaussmeter and a HP 5350B microwave counter. Spectra simulation was performed using in-house software.[25] ^{1}H NMR spectra were taken on a Bruker AC 250 spectrometer; infrared spectra were obtained using a Perkin-Elmer Paragon 1000 PC instrument. Resonance Raman spectra were obtained for KNO_3 pellets by excitation with the lines of an SP 2016 Ar^+ laser or by a CR-590 dye laser employing Coumarine 6 or Rhodamine 6G dyes pumped by the Ar^+ laser. The spectra were recorded by a Dilor XY spectrometer. UV/vis/NIR absorption spectra were recorded on Shimadzu UV160 and Bruins Instruments Omega 10 spectrophotometers. A Perkin-Elmer LS 50 B fluorescence spectrometer served to record emission spectra. Cyclic voltammetry was carried out at 200 mV/s scan rate in dmf/0.1 M Bu_4NPF_6 using a three-electrode configuration (glassy carbon working electrode, Pt counter electrode, Ag/AgCl reference) and a PAR 273 potentiostat and function generator. The ferrocene/ferrocenium couple served as internal reference. Spectroelectrochemical measurements were performed using an optically transparent thin-layer electrode (OTTLE) cell[26] for UV/vis spectra and a two-electrode capillary for EPR studies.[27]

(bpym)$PtCl_2$ (1). This compound has been prepared in analogy to previous reports.[2,4] Elemental analysis, IR, and ^{1}H NMR data

(8) Lippert, B., Ed. *Cisplatin*; Wiley-VCH: Weinheim, Germany, 1999.
(9) (a) Choi, S.; Filotto, C.; Bisanzo, M.; Delaney, S.; Lagasee, D.; Whitworth, J. L.; Jusko, A.; Li, C.; Wood, N. A.; Willingham, J.; Schwenker, A.; Spaulding, K. *Inorg. Chem.* **1998**, *37*, 2500. (b) Collins, J. G.; Rixon, R. M.; Aldrich-Wright, J. R. *Inorg. Chem.* **2000**, *39*, 4377. (c) Mock, C.; Puscasu, I.; Rauterkus, M. J.; Tallen, G.; Wolff, J. E. A.; Krebs, B. *Inorg. Chim. Acta* **2001**, *319*, 109.
(10) (a) Johansson, L.; Tilset, M. *J. Am. Chem. Soc.* **2001**, *123*, 739. (b) Fang, X., Scott, B. L.; Watkin, J. G.; Kubas, G. J. *Organometallics* **2000**, *19*, 4193.
(11) (a) Periana, R. A.; Taube, D. J.; Gamble, S.; Taube, H.; Satoh, T.; Fujii, H. *Science* **1998**, *280*, 560. (b) Gilbert, T. M.; Hristov, I.; Ziegler, T. *Organometallics* **2001**, *20*, 1183. (c) Kua, J.; Xu, X.; Periana, R. A.; Goddard, W. A., III. *Organometallics* **2002**, *21*, 511. (d) Mylvaganam, K.; Bacskay, G. B.; Hush, N. S. *J. Am. Chem. Soc.* **2000**, *122*, 2041.
(12) Bruce, J.; Johnson, D.; Cordes, W.; Sadoski, R. *J. Chem. Crystallogr.* **1997**, *27*, 695.
(13) Klein, A.; Kaim, W.; Fiedler, J.; Zalis, S. *Inorg. Chim. Acta* **1997**, *264*, 269.
(14) Klein, A.; McInnes, E. J. L.; Scheiring, T.; Zalis, S. *J. Chem. Soc., Faraday Trans.* **1998**, *94*, 2979.
(15) Braterman, P. S.; Song, J.-I.; Vogler, C.; Kaim, W. *Inorg. Chem.* **1992**, *31*, 222.
(16) Baumann, F.; Stange, A.; Kaim, W. *Inorg. Chem. Commun.* **1998**, *1*, 305.
(17) Kaim, W.; Reinhardt, R.; Greulich, S.; Sieger, M.; Klein; A.; Fiedler, J. *Collect. Czech. Chem. Commun.* **2001**, *66*, 291.
(18) Kaim, W.; Kohlmann, S. *Inorg. Chem.* **1990**, *29*, 2909.
(19) Kaim, W.; Kohlmann, S. *Inorg. Chem.* **1987**, *26*, 68.
(20) Klein, A.; Hasenzahl, S.; Kaim, W.; Fiedler, J. *Organometallics* **1998**, *17*, 3532.
(21) Kaim, W.; Klein, A.; Glöckle, M. *Acc. Chem. Res.* **2000**, *33*, 755.
(22) Kaim, W. *Inorg. Chem.* **1984**, *23*, 3365.
(23) Braterman, P. S.; Song, J.-I.; Kohlmann, S.; Vogler; C.; Kaim, W. *J. Organomet. Chem.* **1991**, *411*, 207.
(24) Kaim, W.; Kohlmann, S.; Lees, A. J.; Snoeck, T. L.; Stufkens, D. J.; Zulu, M. M. *Inorg. Chim. Acta* **1993**, *210*, 159.
(25) (a) Mabbs, F. E.; Collison, D. *Mol. Phys. Rep.* **1999**, *26*, 39. (b) Mabbs, F. E.; Collison, D. *Electron Paramagnetic Resonance of d Transition Metal Compounds*; Elsevier: Amsterdam, 1992; Chapters 7 and 16.
(26) Krejcik, M.; Danek, M.; Hartl, F. *J. Electroanal. Chem.* **1991**, *317*, 179.
(27) Kaim, W.; Ernst, S.; Kasack, V. *J. Am. Chem. Soc.* **1990**, *112*, 173.

Table 1. Crystallographic Data for **1**

chem formula	$C_8H_6Cl_2N_4Pt$
fw	424.15
space group	monoclinic, $P2_1/c$ (No. 14)
T (K)	293(2)
a (Å)	15.201(1)
b (Å)	20.763(2)
c (Å)	6.7942(5)
β (deg)	102.906(8)
V (Å^3)	2090.28(7)
Z	8
ρ_{calcd} (g cm^{-3})	2.696
μ (mm^{-1})	13.90
λ (Å)	0.710 69
final R [$I > 2\sigma(I)$]	$R_1 = 0.0346$
final R (all data)[a]	$R_w = 0.0503$

[a] $R_1 = (\Sigma||F_o| - |F_c||)/\Sigma|F_o|$. $R_w = \{\Sigma[w(|F_o|^2 - |F_c|^2)^2]/\Sigma[w(F_o^2)^2]\}^{1/2}$.

and diffraction studies of the orange-red dmf solvate[12] and of the red solvent-free form confirmed the identity of the product. Solvent-free **1** was obtained in single crystal form through slow evaporation from a dmf solution at elevated temperature (320 K).

(μ-bpym)[PtCl$_2$]$_2$ (2). A suspension of 500 mg (1.18 mmol) of (bpym)PtCl$_2$ in 100 mL of CH_3NO_2 was treated with 3.98 g (9.43 mmol) of (DMSO)$_2$PtCl$_2$ and heated to 80 °C for 72 h. The orange-brown solid was collected through filtration, washed with 100 mL of CH_2Cl_2, and dried under vacuum to yield 706 mg (86%) of the poorly soluble product. IR (KBr): ν = 3094 (m), 3062 (m), 1587 (m), 1414 (vs), 1383 (w), 1136 (m), 1046 (w), 810 (m), 715 (s), 373 (m), 341 (m) cm^{-1}. Anal. Calcd for $C_8H_6Cl_4N_4Pt_2$ (M_r = 690.14): C, 13.92; H, 0.88; N, 8.12. Found: C, 14.17; H, 0.88; N, 8.12.

Crystallography. Solvent-free single crystals of **1** were grown from a solution in dmf through slow evaporaton at 320 K. The crystals gave the appearance of an orthorhombic unit cell with a base-centered Bravais lattice (e.g. a = 6.7942(5), b = 20.7634-(16), and c = 29.635(2) Å for the *B*-centered case), obviously due to merohedral twinning. However, the transfomation matrix [1/2 0 1/2, 0 1 0, −1 0 0] readily generates the correct monoclinic unit cell (see Table 1). Data were collected of a red specimen (0.1 × 0.05 × 0.05 mm) with a STOE IPDS diffractometer. The structure was solved using direct methods with refinement by full-matrix least squares of F^2, employing the programs SHELXS 86 and SHELXL 93.[28,29] All non-hydrogen atoms were refined anisotropically; hydrogen atoms were introduced at appropriate positions.

DFT Calculations. Ground-state electronic structure calculations of **1**, **2**, and their radical anions have been performed through density-functional theory (DFT) methods using the ADF2000[30,31] and Gaussian98[32] program packages. The lowest excited states of the neutral complexes were calculated by the time-dependent DFT (TD-DFT) method. The Gaussian 98 program was also used for the calculations of vibration frequencies and Raman intensities.

Within Gaussian 98, quasirelativistic effective core pseudopotentials and corresponding optimized sets of basis functions[33] were used for the Pt and Cl centers. Dunning's[34] valence double-ζ functions with polarization were used for the H, C, and N atoms. The "Becke-3-LYP" (B3LYP) potential has been employed.[35] Within the ADF program Slater type orbital (STO) basis sets of double-ζ for H and triple-ζ quality with polarization functions for C, N, Cl, and Pt were employed. The inner shells were represented by a frozen core approximation; viz., 1s for C and N, 1s−2p for Cl, and 1s−4d for Pt were kept frozen. The following density functionals were used within ADF: a local density approximation (LDA) with VWN parametrization of electron gas data and a functional including Becke's gradient correction[36] to the local exchange expression in conjunction with Perdew's gradient correction[37] to the LDA expression (BP). The scalar relativistic (SR) zero-order regular approximation (ZORA) was used within this study. The **g** matrix was obtained from a spin-nonpolarized wave function after incorporating spin−orbit (SO) coupling, using a triple-ζ basis within the frozen core approximation. **A** matrices were obtained from spin-unrestricted wave functions using a quadruple-ζ basis including core electrons.[38] **A** and **g** matrices were obtained by first-order perturbation theory from the ZORA Hamiltonian in the presence of a time-independent magnetic field.[39]

To examine the possible deviation from planarity the geometry optimization and vibrational analysis of **1** and **2** were done without any symmetry constraints. Frequency calculations were done for G98/B3LYP-optimized geometries which involve essentially planar molecules **1** and **2**. The scaling factor for vibrations calculated with the B3LYP functional and double-ζ basis was set at 0.963.[40] Since the deviations of the optimized structures from ideal higher symmetry are small, single point calculations for **1** and **2** were performed in C_{2v} or D_{2h} constrained optimized structures, respectively. Within both systems, the bpym ligand defines the *xy* plane and the Pt atoms lie on the *x* axis. To estimate the possible response of electronic structure due to the solvation, the solvent was modeled in ADF/BP calculations by the conductor-like screening model (COSMO) or by the polarized continuum model (PCM) implemented in G98.[41]

Results and Discussion

Synthesis. The new dinuclear (μ-bpym)[PtCl$_2$]$_2$ (**2**) was obtained as a sparingly soluble yellow material from the

(28) Sheldrick, G. M. *SHELXS-86, Program for Crystal Structure Analysis*; Universität Göttingen: Göttingen, Germany, 1986.
(29) Sheldrick, G. M. *SHELXL-93, Program for Crystal Structure* Analysis; Universität Göttingen: Göttingen, Germany, 1993.
(30) Fonseca Guerra, C.; Snijders, J. G.; Te Velde, G.; Baerends, E. J. *Theor. Chem. Acc.* **1998**, *99*, 391.
(31) van Gisbergen, S. J. A.; Snijders, J. G.; Baerends, E. J. *Comput. Phys. Commun.* **1999**, *118*, 119.
(32) Frisch, M. J.; Trucks, G. W.; Schlegel, H. B.; Scuseria, G. E.; Robb, M. A.; Cheeseman, J. R.; Zakrzewski, V. G.; Montgomery, J. A.; Stratmann, R. E.; Burant, J. C.; Dapprich, S.; Millam, J. M.; Daniels, A. D.; Kudin, K. N.; Strain, M. C.; Farkas, O.; Tomasi, J.; Barone, V.; Cossi, M.; Cammi, R.; Mennucci, B.; Pomelli, C.; Adamo, C.; Clifford, S.; Ochterski, J.; Petersson, G. A.; Ayala, P. Y.; Cui, Q.; Morokuma, K.; Malick, D. K.; Rabuck, A. D.; Raghavachari, K.; Foresman, J. B.; Cioslowski, J.; Ortiz, J. V.; Stefanov, B. B.; Liu, G.; Liashenko, A.; Piskorz, P.; Komaromi, I.; Gomperts, R.; Martin, R. L.; Fox, D. J.; Keith, T.; Al-Laham, M. A.; Peng, C. Y.; Nanayakkara, A.; Gonzalez, C.; Challacombe, M.; Gill, P. M. W.; Johnson, B. G.; Chen, W.; Wong, M. W.; Andres, J. L.; Head-Gordon, M.; Replogle, E. S.; Pople, J. A. *Gaussian 98*, revision A.7; Gaussian Inc.: Pittsburgh, PA, 1998.
(33) Andrae, D.; Haeussermann, U.; Dolg, M.; Stoll, H.; Preuss, H. *Theor. Chim. Acta* **1990**, *77*, 123.
(34) Woon, D. E.; Dunning, T. H., Jr. *J. Chem. Phys.* **1993**, *98*, 1358.
(35) Stephens, P. J.; Devlin, F. J.; Cabalowski, C. F.; Frisch, M. J. *J. Phys. Chem.* **1994**, *98*, 11623.
(36) Becke, A. D. *Phys. Rev. A* **1988**, *38*, 3098.
(37) Perdew, J. P. *Phys. Rev. A* **1986**, *33*, 8822.
(38) van Lenthe, E.; Ehlers, A.; Baerends, E. J. *J. Chem. Phys.* **1999**, *110*, 8943.
(39) (a) van Lenthe, E.; van der Avoird, A.; Wormer, P. E. S. *J. Chem. Phys.* **1998**, *108*, 4783. (b) van Lenthe, E.; van der Avoird, A.; Wormer, P. E. S. *J. Chem. Phys.* **1997**, *107*, 2488.
(40) Wong, M. W. *Chem. Phys. Lett.* **1996**, *256*, 391.
(41) (a) Klamt, A.; G. Schürmann, *J. Chem. Soc., Perkin Trans.* **1999**, 799. (b) Amovilli, C.; Barone, V.; Cammi, R.; Cances, E.; Cossi, M.; Mennucci, B.; Pomelli, C. S.; Tomasi, J. *Adv. Quantum Chem.* **1999**, *32*, 227.

Table 2. Selected Bond Lengths (Å) and Angles (deg) for the Molecules in the Crystal of **1**[a]

Pt1−N1	1.983(10)	Pt2−N5	1.984(9)
Pt1−N2	2.015(9)	Pt2−N6	1.995(10)
Pt1−Cl1	2.286(3)	Pt2−Cl3	2.278(3)
Pt1−Cl2	2.291(4)	Pt2−Cl4	2.289(4)
C1−C2	1.48(2)	C9−C10	1.48(2)
N1−Pt1−N2	78.7(5)	N5−Pt2−N6	80.9(5)
N1−Pt1−Cl1	174.4(4)	N5−Pt2−Cl3	175.1(4)
N2−Pt1−Cl1	95.9(3)	N6−Pt2−Cl3	94.3(3)
N1−Pt1−Cl2	96.1(4)	N5−Pt2−Cl4	95.4(4)
N2−Pt1−Cl2	173.9(3)	N6−Pt2−Cl4	176.2(3)
Cl1−Pt1−Cl2	89.43(13)	Cl3−Pt2−Cl4	89.45(13)

[a] For numbering, compare Figure 1.

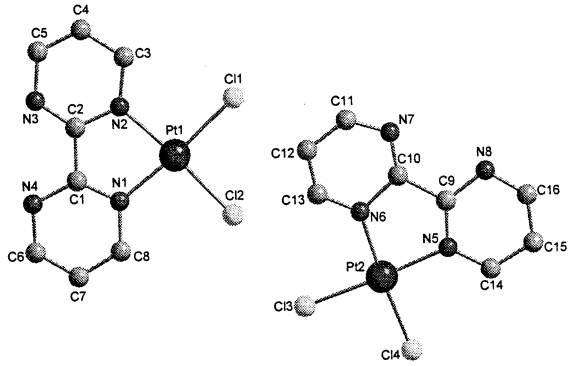

Figure 1. Molecular structures and atomic numbering of the two independent molecules in the unit cell of solvent-free **1**.

prolonged reaction of mononuclear (bpym)$PtCl_2$ (**1**) [2,4,11a,12] with $(DMSO)_2PtCl_2$ in nitromethane. Analytical, spectroscopic, and electrochemical data (cf. below) confirm its identity in relation to **1**. Although it certainly requires some activation to add a second metal complex fragment to the mononuclear (bpym)$PtCl_2$ molecule[4,12] with its typically[2,17] larger "backside" N----N bite in comparison to N--Pt--N, there is no intrinsic problem in obtaining stable dinuclear complexes of platinum metal or other transition metal fragments with the bpym bridging ligand.[16,17,42] Any loss in basicity at the free nitrogen atoms of the bpym ligand in **1** through the σ acceptor effect of $PtCl_2$ may be offset by back-donation from occupied metal d orbitals. The slow reactivity of platinum precursor compounds may have prevented the synthesis of **2** in the past.[2]

Structural Aspects. In addition to two previous crystal structure reports on **1**·0.5nmp (nmp = 1-methyl-2-pyrrolidinone)[4] and **1**·dmf (dmf = *N*,*N*-dimethylformamide)[12] we have now obtained crystals of the solvent-free mononuclear complex (bpym)$PtCl_2$ (Table 1). Whereas the intramolecular structure parameters (Table 2) of the two independent molecules (Figure 1) in the solvent-free crystals are unsurprising and essentially as observed before[4,12] and calculated by DFT (see Table 3), the arrangement of molecules exhibits an interesting variation to a much studied theme:[1,2,4,5,12,43,44]

Table 3. Selected ADF/BP Calculated Bond Lengths (Å) and Angles (deg) of [Pt(bpym)Cl_2] (**1**), [Cl_2Pt(bpym)$PtCl_2$] (**2**) and Their Radical Anions[a]

	1	**1**$^{\bullet-}$	**2**	**2**$^{\bullet-}$
Pt−N	2.017	2.011	2.047	2.040
Pt−Cl	2.289	2.330	2.297	2.305
N_1-C_6	1.354	1.341	1.354	1.339
N_1-C_2	1.372	1.409	1.357	1.383
N_3-C_2	1.330	1.361	1.357	1.383
N_3-C_4	1.339	1.324	1.354	1.339
C_4-C_5	1.386	1.392	1.394	1.403
C_5-C_6	1.398	1.412	1.394	1.403
C_2-C_2'	1.472	1.420	1.427	1.386
N_1-Pt-N_2	80.0	80.6	80.9	81.9
Cl−Pt−Cl	90.7	90.0	92.7	91.9
$Pt-N_1-C_6$	126.7	126.9	130.5	131.5
$Pt-N_1-C_2$	115.9	114.9	112.6	111.2
$N_1-C_2-C_2'$	114.1	114.8	117.0	117.9
$N_1-C_2-N_3$	125.1	122.7	126.1	124.3
$N_3-C_2-C_5$	120.8	122.5	117.0	117.9

[a] Numbering (subscripts) according to heterocyclic nomenclature.

the two independent molecules in the unit cell undergo two different kinds of stacking aggregation (Figure 2). Molecule A (with Pt1) exhibits some similarity with the red form of (bpy)Pt$(NCS)_2$.[4] One six-membered ring of each molecule A appears to engage in partial π/π interaction with another such ring from the complex A in the next layer. As a result, the vectors bisecting the individual molecules A form an approximately 120° angle φ (ca. 137° rotation in (bpy)-Pt$(NCS)_2$[4]). The Pt1--Pt1 distance is 3.505 Å, and the Pt1--Pt1--Pt1 zigzag angle 151.5°. A more linear arrangement (170.0°) with closer metal−metal contacts of 3.299 Å was observed for (bpy)Pt$(NCS)_2$.[4] Molecules B (with Pt2), on the other hand, are related to the red forms of (bpy)$PtCl_2$,[1,5] (bpym)Pt$(CN)_2$·dmf,[44] and (bpym)$PtCl_2$·solvent.[4,12] The aforementioned vectors are antiparallel (φ = 180°), and there is no overlap of the six-membered rings. The Pt2--Pt2 distances of 3.434 and 3.466 Å and the Pt2--Pt2--Pt2 angle of 159.9° in the stack are in the range reported previously for chloride-containing "red forms".[1,4,5,12]

The availability of catalytically relevant[11c] free basic nitrogen atoms in **1** allows for weak intermolecular (interstack) C−H--N interactions in the crystal as illustrated by a relatively short distance of 3.357 Å between C4 (from molecule A) and N8 (from molecule B) with an approximate C−H--N angle of 176.5°. This additional interaction may be responsible for the occurrence and coexistence of two kinds of stacks within the same crystal structure. Interstack Pt1--Pt2 distances are larger than 7.9 Å.

The structurally observed intermolecular C−H--N interaction suggests that the free nitrogen atoms are still rather basic, probably because of back-donation from the platinum(II) atom. In the catalytic cycle suggested for methane activation by **1** as a precursor in hot sulfuric acid,[11] the proposed loss of a chloride ligand would leave a cationic platinum(II) center which could not provide as much electron density for back-donation to bpym. Even then, however, such a mononuclear

(42) (a) Vogler, C.; Hausen, H.-D.; Kaim, W.; Kohlmann, S.; Kramer, H. E. A.; Rieker, J. *Angew. Chem.* **1989**, *101*, 1734; *Angew. Chem., Int. Ed. Engl.* **1989**, *28*, 1659. (b) Schwach, M.; Hausen H.-D.; Kaim, W. *Chem.—Eur. J.* **1996**, *2*, 446.
(43) Canty, A. J.; Skelton, B. W.; Traill, P. R.; White, A. H. *Aust. J. Chem.* **1992**, *45*, 417.
(44) (a) Biedermann, J.; Gliemann, G.; Klement, U.; Range, K.-J.; Zabel, M. *Inorg. Chim. Acta* **1990**, *171*, 35. (b) Biedermann, J.; Gliemann, G.; Klement, U.; Range, K.-J.; Zabel, M. *Inorg. Chim. Acta* **1990**, *169*, 63.

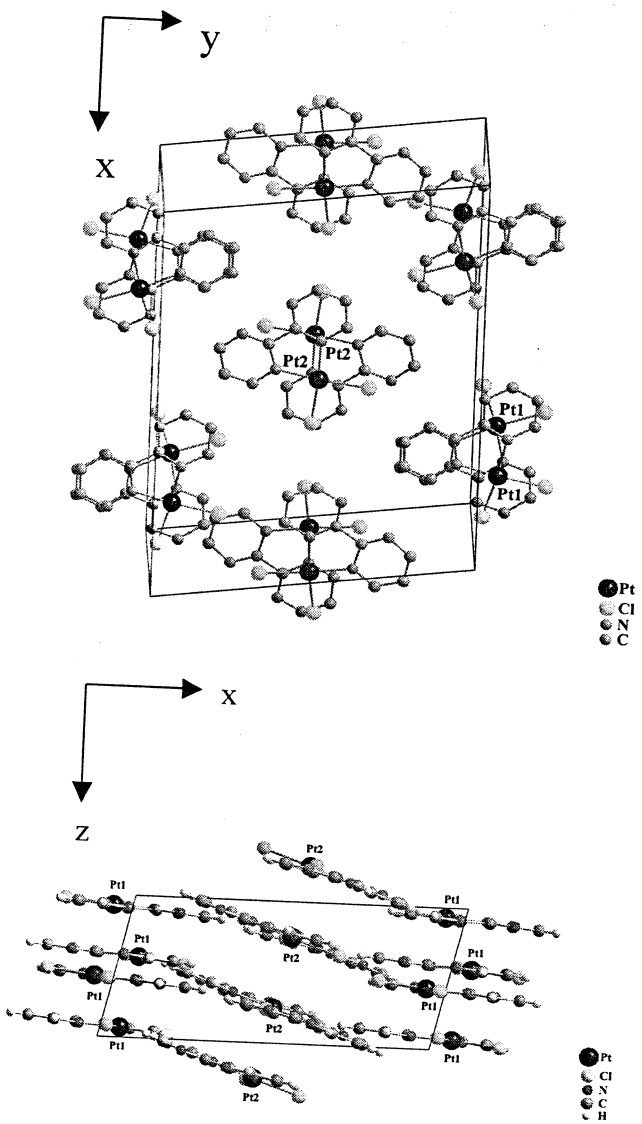

Figure 2. Crystal packing in **1**: Views along the *z* axis (top) and along the *y* axis (bottom).

bpym complex would offer additional binding sites for electrophiles such as H^+ in concentrated H_2SO_4.[11c]

The new dinuclear complex **2** has so far failed to yield single crystals of X-ray-diffraction quality. The DFT calculation (Table 3) predicts an essentially planar structure with very similar bond parameters as for **1**. Significant differences lie in the slightly longer Pt−N bonds for **2** due to the absence of bending along the bpym molecular axis[1,17] (cf. the increase in the angle Pt−N^1−C^6) and in the shortening of the inter-ring C^2−C$^{2'}$ bond.

Reduced State: Cyclic Voltammetry, EPR, and DFT Calculations. Both complexes **1** and **2** are reduced in two well-separated reversible one-electron steps as evident from the cyclic voltammograms obtained in dmf solution (Figure 3). Oxidation processes were not observed up to 1.0 V vs ferrocene. The potentials are listed in Table 4 in comparison to values reported for (μ-bpym)[PtMes$_2$]$_2$ (Mes = mesityl = 2,4,6-trimethylphenyl).[13]

Differences of about 0.7 V between the first and second one-electron addition are typical for bpym and its complexes;[19] the ligand itself has $E_{1/2}$(red1) = −2.24 V and $E_{1/2}$(red2) = −2.95 V.[18,19,45] The strong anodic shift of the reduction potential on single and especially double coordination illustrates the σ-acceptor capacity of [PtCl$_2$]. In contrast to the −1.18 V for (μ-bpym)[PtMes$_2$]$_2$, −1.32 V for (μ-bpym)[PtMe$_2$]$_2$, and −1.34 V for (μ-bpym)[PtMe$_4$]$_2$,[13] the −0.65 V value for **2** further supports this notion of [PtCl$_2$] as being a superb σ-acceptor.

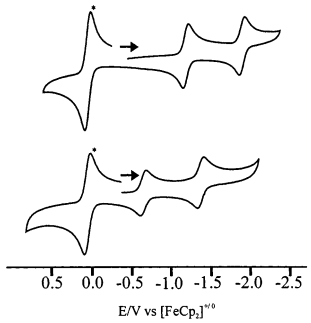

Figure 3. Cyclic voltammograms of **1** (top) and **2** (bottom) in dmf/0.1 M Bu_4NPF_6 (ferrocene standard indicated by an asterisk).

A comparison with other 5d metal halide dimers bridged by bpym as shown in Table 5 reveals similarities and differences.

Whereas the potentials for the reversible first electron uptake to a bpym$^{\bullet-}$-bridged compound are rather similar (Table 5), the chloro complexes containing rhenium(I),[18,23] osmium(II),[16] and iridium(III)[17] but not platinum(II) exhibit an irreversible second reduction due to chloride dissociation.[16,17] In addition to an intrinsic stability of the platinum(II)−chloride bond, we attribute this difference to the planar situation at the Pt^{II}N$_2$Cl$_2$ center with its 5d^8 configuration; the other systems mentioned above have a 5d^6 configuration with the metal−halide bond not in the π plane but largely perpendicular to it. According to simple orbital models[46,47] this arrangement would favor dissociation through π^*/σ^* conjugative interaction. The controlled reductive dissociation of transition metal-to-chloride bonds is essential for catalytic processes such as the rhenium-catalyzed CO_2 reduction[48] or the rhodium- or iridium-centered hydride generation.[49,50]

In situ generation of the radical anion complexes **1**$^{\bullet-}$ and **2**$^{\bullet-}$ allowed us to study the EPR properties of these intermediates in fluid and glassy frozen solution (Figures 4 and 5). X band measurements provided sufficient resolution of the hyperfine-split g components, in contrast to other platinum metal radical compounds where high-frequency EPR is necessary.[51] The data as obtained from simulations are summarized in Table 4, again in comparison with those

(45) Ernst, S.; Kaim, W. *J. Am. Chem. Soc.* **1986**, *108*, 3578.
(46) Klein, A.; Vogler, C.; Kaim, W. *Organometallics* **1996**, *15*, 236.
(47) Kaim, W.; Olbrich-Deussner, B.; Gross, R.; Ernst, S.; Kohlmann, S.; Bessenbacher, C. In *Importance of Paramagnetic Organometallic Species in Activation, Selectivity and Catalysis*; Chanon, M., Ed.; Kluwer Academic Publishers: Dordrecht, The Netherlands, 1989; p 283.
(48) (a) Hawecker, J.; Lehn, J.-M.; Ziessel, R. *J. Chem. Soc., Chem. Commun.* **1983**, 536. (b) Hawecker, J.; Lehn, J.-M.; Ziessel, R. *Helv. Chim. Acta* **1986**, *69*, 1990.
(49) Kölle, U.; Grätzel, M. *Angew. Chem.* **1987**, *99*, 572; *Angew. Chem., Int. Ed. Engl.* **1987**, *26*, 568.
(50) Ziessel, R. *J. Am. Chem. Soc.* **1993**, *115*, 118.

Table 4. Electrochemical[a] and Spectroscopic Data[b,c] of the Complexes

	$[(bpym)PtX_2]^n$		$\{(\mu\text{-bpym})[PtX_2]_2\}^n$	
	X = Cl	X = Mes[d]	X = Cl	X = Mes[e]
$E_{1/2}$(red1)[a]	−1.28(66)	−1.67(61)	−0.65(58)	−1.18(84)
$E_{1/2}$(red2)[a]	−2.01(70)	−2.38(102)	−1.31(76)	−1.92(105)
$\Delta E_{1/2}$(red)	0.73	0.71	0.66	0.74
		EPR[b]		
g_1	2.034	2.0291	2.049	2.0435
g_2	2.005	2.0051	2.008	2.0091
g_3	1.938	1.9453	1.902	1.916
$g_1 - g_3$	0.096	0.0838	0.147	0.1275
g_{iso}	1.9910	1.9927	1.9862	1.9915
A_1	5.0	3.6	3.9	<2.5
A_2	6.9[f]	≈3.0	5.1[g]	1.6
A_3	≤3.0	<2.5	⩽3.0	<2.0
A_{iso}	4.6	3.0	3.7	<2.5
		UV−Vis[c]		
λ_{max}/ϵ ($n = 0$)	470 sh, 402/2200, 390 sh, 365 sh, 300/7200	491/1500, 423 sh	550 br, 465/3300, 435/3200, 400 sh, 345 sh, 315/12400	627/3000, 432/6300, 375/10000, 362
λ_{max} ($n = 1$)	1020 sh, 910; 483, 452, 425; 350 sh	1150 sh, 950, 828; 506, 477, 453 sh; 356 sh	450, 425 sh; 340 sh, 315[h]	899, 610 sh, 488
λ_{max} ($n = 2$)	360 sh, 320	377	1030, 870; 360 sh, 305	n.a.

[a] From cyclic voltammetry in dmf/0.1 M Bu_4NPF_6 (X = Cl) or THF/0.1 M Bu_4NPF_6 (X = Mes). Potentials in V vs ferrocenium/ferrocene; peak potential differences in mV (in parentheses). [b] EPR spectra from in situ reduction in dmf/0.1 M Bu_4NPF_6 (X = Cl) or DCE/0.1 M Bu_4NPF_6 (X = Mes). ^{195}Pt hyperfine coupling constants A in mT. [c] Absorption maxima in nm from OTTLE spectroelectrochemistry measurements in dmf/0.1 M Bu_4NPF_6 (X = Cl), THF/0.1 M Bu_4NPF_6 (X = Mes, mononuclear complex) or DCE/0.1 M Bu_4NPF_6 (X = Mes, dinuclear complex). Molar extinction coefficients ϵ in M^{-1} cm^{-1}. [d] Reference 7c. [e] Reference 13. [f] $A(^1H) = 0.7$ mT (2H). [g] $A(^1H) = 0.75$ mT (2H). [h] Long-wavelength band not observable due to low signal-to-noise ratio (poor solubility).

Table 5. Electrochemical,[a] EPR,[b] and UV−Vis Absorption Data[c] for Radical Complexes $[(\mu\text{-bpym}^{\bullet-})[L_nClM]_2\}^k$

	L_nClM			
	$(OC)_3ClRe$	$(\eta^6\text{-}p\text{-Cym})ClOs^+$	$(\eta^5\text{-}C_5Me_5)ClIr^+$	Cl_2Pt
$E_{1/2}$(ox)[a]	−1.01[d]	−0.66	−0.74[e]	−0.65
$E_{1/2}$(red)[a]	irr[f]	irr[f]	irr[f]	−1.31
		EPR[b]		
g_1	n.a.	2.0076	2.0029	2.049
g_2	n.a.	1.9962	1.9849	2.008
g_3	n.a.	1.9739	1.9451	1.902
$g_1 - g_3$	n.a.	0.0337	0.0578	0.147
g_{iso}	2.0005[g]	1.9926	1.9778	1.9862
A_{iso}[h]	≈1.2[g]	1.2	n.o.	3.7
A_{iso}/a_o[i]	1×10^{-3}	2.5×10^{-3}	n.o.	3.0×10^{-3}
		UV−Vis[c]		
λ_{max}[j]	444	466	510	450
ref	18, 23	16	17	this work

[a] From cyclic voltammetry in dmf/0.1 M Bu_4NPF_6. Potentials in V vs ferrocenium/ferrocene. [b] EPR spectra from in situ reduction in dmf/0.1 M Bu_4NPF_6. ^{195}Pt hyperfine coupling constants A in mT. [c] Absorption maxima in nm from OTTLE spectroelectrochemistry measurements in dmf/0.1 M Bu_4NPF_6. Extinction coefficients not determined for X = Cl because of low solubility. [d] Converted from −0.51 V vs SCE: Juris, A.; Campagna, S.; Bidd. I.; Lehn, J.-M.; Ziessel, R. *Inorg. Chem.* **1988**, *27*, 4007. [e] Low-temperature measurements (−15 °C). [f] Dissociation of chloride. [g] Measurement in acetone. [h] $^{185,187}Re$ ($I = 5/2$, $a_o \approx 1260$ mT), ^{189}Os ($I = 3/2$, $a_o = 471$ mT), ^{195}Pt ($I = 1/2$, $a_o = 1228$ mT). [i] Isotropic hyperfine constant a_o from ref 37. [j] Main band in the visible region ($\pi(7) \rightarrow \pi(10)$).[23]

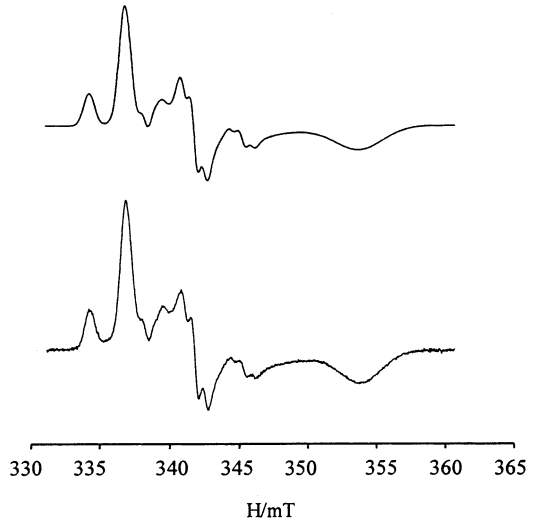

Figure 4. EPR spectrum of electrolytically generated $\mathbf{1}^{\bullet-}$ in dmf/0.1 M Bu_4NPF_6 at 110 K (bottom) and computer simulation (top).

of the mononuclear and dinuclear dimesitylplatinum analogues.

The dichloroplatinum(II) radical species exhibit higher g anisotropies $g_1 - g_3$, lower g_{iso} values, and larger ^{195}Pt hyperfine coupling constants than the $[PtMes_2]$ analogues. While the EPR results for mononuclear $\mathbf{1}^{\bullet-}$ are expectedly close to those of $[(bpy)PtCl_2]^{\bullet-}$,[6] the dinuclear $\mathbf{2}^{\bullet-}$ is distinguished by a g anisotropy which is remarkably large for a radical complex. Both the g and the A values signify considerable metal participation at the singly occupied MO; however, the alternative mixed-valent resonance structure $[Cl_2Pt^{I}(\mu\text{-bpym})Pt^{II}Cl_2]^{\bullet-}$ is still considered to have only a minor contribution in comparison to $[Cl_2Pt^{II}(\mu\text{-bpym}^{-I})\text{-}Pt^{II}Cl_2]^{\bullet-}$. The hyperfine coupling in $\mathbf{2}^{\bullet-}$ indicates equivalence of the two Pt centers. For a delocalized mixed-valent situation ($Pt^{1.5}/Pt^{1.5}$), one would expect $A(\mathbf{1}^{\bullet-}) = 2A(\mathbf{2}^{\bullet-})$.[52] In fact, the ^{195}Pt coupling is only about 30% higher in the mononuclear compound (Table 4), confirming the still predominant

(51) Frantz, S.; Hartmann, H.; Doslik, N.; Wanner, M.; Kaim, W.; Kümmerer, H.-J.; Denninger, G.; Barra, A.-L.; Duboc-Toia, C.; Fiedler, J.; Ciofini, I.; Urban, C.; Kaupp, M. *J. Am. Chem. Soc.*, in press.

(52) (a) Gross, R.; Kaim, W. *Inorg. Chem.* **1986**, *25*, 4865. (b) Kaim, W.; Bruns, W.; Poppe, J.; Kasack, V. *J. Mol. Struct.* **1993**, *292*, 221.

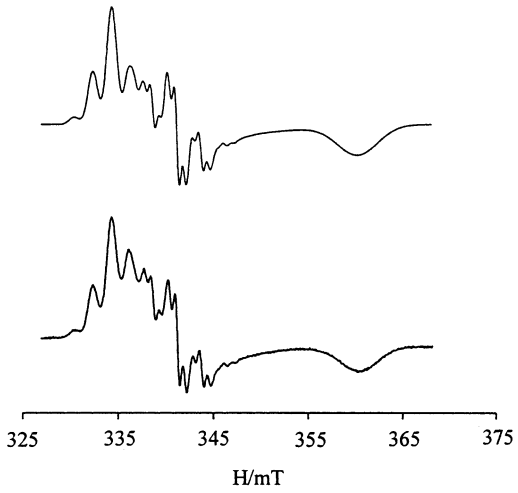

Figure 5. EPR spectrum of electrolytically generated **2**$^{\bullet-}$ in dmf/0.1 M Bu_4NPF_6 at 110 K (bottom) and computer simulation (top).

radical character of the species. This notion is also supported by the observation of a ^{1}H coupling of about 0.7 mT for the central g components in **1**$^{\bullet-}$ and **2**$^{\bullet-}$; in agreement with previous HMO calculations[22] we attribute this splitting to the $H^{5,5'}$ protons of the bpym$^{\bullet-}$ ligand.

The particularly large g anisotropy and metal hyperfine coupling constant for **2**$^{\bullet-}$ are also evident (Table 5) from a comparison with other 5d metal halide dimers bridged by the 2,2′-bipyrimidine radical anion.[16−18] Besides better orbital mixing for increased metal contribution, the higher spin−orbit coupling factor ζ[53] of platinum(II) in comparison to osmium(II) and rhenium(I) will play an important role. Concerning the deviation of g from g(electron) = 2.0023, the high ζ value for trivalent iridium is apparent from g_{iso} = 1.9778,[17] which lies even lower than that of **2**$^{\bullet-}$ (Table 5).

For a confirmation and quantification of the above arguments we have used DFT methodology to calculate the structures and EPR properties of **1**$^{\bullet-}$ and **2**$^{\bullet-}$. The structural parameters are listed in Table 3 together with those of the nonreduced molecules. Changes in electron acquisition affect predominantly the bpym ligand, especially through the characteristic shortening of the inter-ring bond C^2-$C^{2'}$.

The composition of the ADF/BP-calculated frontier molecular orbitals of [Pt(bpym)Cl$_2$] is given in Table 6. The close-lying HOMOs 8b$_1$, 21a$_1$, and 6a$_2$ are mainly formed by combinations of Cl orbitals with Pt d orbitals. The MOs 20a$_1$ and 17b$_2$ below this set of orbitals are Pt or Cl localized, respectively. The contribution of bpym π MOs to these orbitals is 18% or lower. The LUMO, 9b$_1$, has the same character as the lowest unoccupied π* orbital of the free bpym ligand,[24] slightly perturbed by a small contribution (6%) from the d_{xz} Pt orbital. The next two higher lying unoccupied molecular orbitals correspond mainly to higher π* orbitals of bpym.[24] An analogous sequence of frontier MOs is obtained for **2** (Table 7). Here the metal-localized orbitals are characterized as pairs of orbitals that correspond to the symmetrical or antisymmetrical combination of PtCl$_2$ fragment orbitals. The LUMO is also mainly formed by the π* orbital of the free bpym ligand, each Pt center contributing by about 5% to this MO. Note that the calculated relative energies of the LUMOs of **1** and **2** are consistent with the reduction potentials. The CH_2Cl_2 solvent effect modeled by the COSMO procedure affects mainly the composition of these HOMOs with large Cl contributions. When the solvent effect is introduced, the Cl contributions within **1** diminish to 39%, 49%, and 34% in orbitals 8b$_1$, 21a$_1$, and 6a$_2$, respectively. In addition, the HOMO orbitals exhibit larger Pt character and the HOMO−LUMO separation increases. The LUMO character, in the other hand, does not change substantially. The corresponding frontier orbitals of **2** are influenced accordingly. Both models of solvation (COSMO within ADF and PCM within G98) enlarge the HOMO−LUMO separation by about 0.5 eV and affect the frontier orbitals comparably.

Table 6. ADF/BP Calculated One-Electron Energies and Percentage Composition of Selected Frontier MOs of **1**, Expressed in Terms of Composing Fragments

MO	E (eV)	predominant character	Pt	bpym	Cl (tot.)
			Unoccupied		
18b$_2$	−2.35	Pt + Cl	46 (d_{yz})	20	33
7a$_2$	−3.32	bpym (π_3*)	3 (d_{xy})	96 (π*)	1
10b$_1$	−3.52	bpym (π_2*)	4 (d_{xz})	95 (π*)	1
9b$_1$	−4.16	bpym (π_1*)	6 (d_{xz})	90 (π*)	3
			Occupied		
6a$_2$	−5.54	Cl + Pt	41 (d_{xy})	4	54
21a$_1$	−5.70	Cl + Pt	25 (d_{z^2}); 11 ($d_{x^2-y^2}$)	13	51
8b$_1$	−5.93	Cl + Pt	35 (d_{xz})	18	46
20a$_1$	−6.20	Pt	18 (s); 23 (d_{z^2}); 53 ($d_{x^2-y^2}$)	2	3
17b$_2$	−6.25	Cl			99
16b$_2$	−7.32	bpym	2 (p_y)	9	89

Table 7. ADF/BP Calculated One-Electron Energies and Percentage Composition of Selected Frontier MOs of **2**, Expressed in Terms of Composing Fragments

MO	E (eV)	predominant character	Pt	bpym	Cl (tot.)
			Unoccupied		
12b$_{3g}$	−2.99	Pt + Cl	48 (d_{yz})	21	34
13b$_{2u}$	−3.45	Pt + Cl	48 (d_{yz})	17	35
5a$_u$	−4.20	bpym (π_3*)	6 (d_{xy})	92 (π*)	2
7b$_{2g}$	−4.39	bpym (π_2*)	9 (d_{xz})	87 (π*)	3
8b$_{3u}$	−5.09	bpym (π_1*)	10(d_{xz})	83 (π*)	6
			Occupied		
5b$_{1g}$	−6.14	Cl + Pt	41 (d_{xy})	2	57
4a$_u$	−6.20	Cl + Pt	36 (d_{xy})	9	55
14b$_{1u}$	−6.30	Cl + Pt	23 (d_{z^2}); 12 ($d_{x^2-y^2}$)	1	64
16a$_{1g}$	−6.31	Cl + Pt	24 (d_{z^2}); 10 ($d_{x^2-y^2}$)	2	63
6b$_{2g}$	−6.50	Cl + Pt	2 (p_x); 35 (d_{xz})	14	49
7b$_{3u}$	−6.70	Cl + Pt	2 (p_x); 34 (d_{xz})	14	49
13b$_{1u}$	−6.83	Pt	16 (s); 22 (d_{z^2}); 54 ($d_{x^2-y^2}$)	2	4
15a$_{1g}$	−6.84	Pt	18 (s); 21 (d_{z^2}); 55 ($d_{x^2-y^2}$)	2	3

The reduction of both complexes leads to the acceptance of the added electron by the predominantly bpym-localized LUMO. Figure 6 shows the composition of the singly occupied MO (SOMO) of **2**$^{\bullet-}$. The SOMO compositions do not substantially differ from those of corresponding LUMOs of the neutral systems. In agreement with the previously reported electronic structure of [Pt(bpy)Cl$_2$]$^{\bullet-}$,[6a−d] the 5d contribution to this orbital is much larger than the 6p contribution. The SOMO contains 6% $5d_{xz}$ and 0.7% $6p_x$ or

(53) Weil, J. A.; Bolton, J. R.; Wertz, J. E. *Electron Paramagnetic Resonance*; Wiley: New York, 1994.

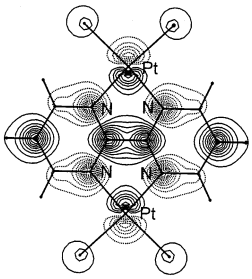

Figure 6. ADF/BP calculated contour map of the SOMO ($8b_{3u}$) of $\mathbf{2}^{\bullet-}$, 0.5 Å over the *xy* plane.

Table 8. Comparison of Experimental and Calculated *g* Values[a] and ^{195}Pt Hyperfine Constants *A* (mT)[b] for Complexes $\mathbf{1}^{\bullet-}$ and $\mathbf{2}^{\bullet-}$

	$\mathbf{1}^{\bullet-}$		$\mathbf{2}^{\bullet-}$	
	expt	calcd	expt	calcd
g_1	2.034	2.076	2.049	2.132
g_2	2.005	1.998	2.008	1.993
g_3	1.938	1.894	1.902	1.820
$g_1 - g_3$	0.096	0.182	0.147	0.312
g_{iso}[e]	1.993	1.989	1.987	1.982
A_1	−5.0	−5.98	−3.9	−4.84
A_2	−6.9	−3.63	−5.1	−3.03
A_3	>−3.0	−2.69	>−3.0	−2.50
A_{iso}	−4.6	−4.10	−3.7	−3.46

[a] Spin-restricted calculations including spin−orbit coupling. [b] Calculations using scalar relativistic UKS-ZORA approach.

5% $5d_{xz}$ and 0.2% $6p_x$ contributions/Pt atom for $[Pt(bpym)Cl_2]^-$ or $[PtCl_2(\mu\text{-bpym})PtCl_2]^-$, respectively. The nonzero metal contribution is reflected by the calculated spin densities on the metal center and by the rather large separation of anisotropic *g* components (Table 8). The spin densities on the individual Pt atoms are 0.053 for $\mathbf{1}^{\bullet-}$ and 0.039 for $\mathbf{2}^{\bullet-}$, reflected by the lower isotropic *A* value for the dinuclear complex. The calculations of *A* values required the inclusion of core electrons. Basis sets with frozen core approximations gave lower *A* values.

The calculated ^{195}Pt coupling constants and *g* component values are summarized in Table 8. These calculations were performed without support by spectral parameters to evaluate current methodology. In relation to the experimental data the calculated values seem to exaggerate the metal contribution to the *g* anisotropy $\Delta g = g_1 - g_3$. Furthermore, the magnitudes of the calculated hyperfine coupling constants are in the order $A_3 < A_2 < A_1$ whereas the experimental observation is $A_3 < A_1 < A_2$. However, both the larger individual hyperfine coupling for $\mathbf{1}^{\bullet-}$ vs $\mathbf{2}^{\bullet-}$ and the higher total participation of the metals at the SOMO in $\mathbf{2}^{\bullet-}$ are reproduced by the DFT calculations. Previous calculations based on EPR spectroscopic data for $[(bpy)PtCl_2]^{\bullet-}$ and related systems[6c,d] used Rieger's semiempirical approach[54] for assigning spin densities to individual centers. A similar analysis in this case gives contributions of 3.6% and 6.5% of the Pt 5d and 6p orbitals, respectively, to the SOMO of $\mathbf{1}^{\bullet-}$. For $\mathbf{2}^{\bullet-}$ contributions of 2.2% 5d and 4.0% 6p from each Pt center are calculated. These are in good agreement with the DFT calculations with the admixture of both the 5d and 6p orbitals from each Pt center decreasing from $\mathbf{1}^{\bullet-}$ to $\mathbf{2}^{\bullet-}$.

(54) Rieger, P. H. *J. Magn. Reson.* **1997**, *124*, 140.

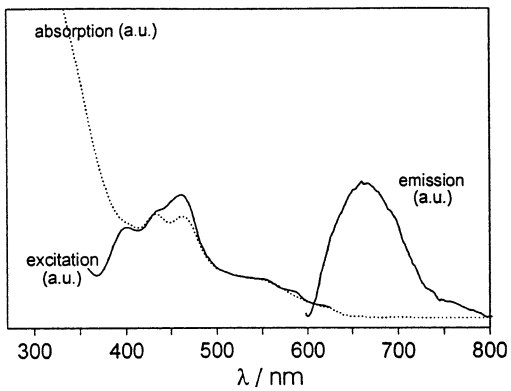

Figure 7. Absorption, emission, and excitation spectra ($\lambda = 700$ nm) of **2** in dmf at room temperature.

Excited State: Absorption, Emission, and Excitation Spectra, Spectroelectrochemistry, and Resonance Raman Spectroscopy. Owing to the stabilized $[PtCl_2]$-centered HOMOs (Tables 6 and 7), both **1** and **2** exhibit metal-to-ligand charge transfer (MLCT) absorptions at comparatively high energies, despite the low-lying π^* MOs as evident from strongly shifted reduction potentials. Both compounds are luminescent.

The absorption spectrum of mononuclear **1** shows an intense long-wavelength band around 400 nm which exhibits slightly negative solvatochromism ($\lambda_{max} = 396$ nm in MeCN, 402 nm in dmf, 413 nm in CH_2Cl_2). A closer look at the low-energy side reveals a very weak shoulder around 470 nm. The dinuclear complex **2** exhibits a band system in dmf solution with maxima at 435 and 465 nm. There is an intense band at 315 nm and a broad feature at the low-energy side around 550 nm. Due to the poor solubility of **2** in most solvents its solvatochromism could not be investigated.

The mononuclear complex shows emission at ambient temperatures. In the solid, the excitation at 480 nm into the weak long-wavelength absorption band leads to a weak and broad emission at 670 nm. Resonance Raman experiments gave essentially the same results. The excitation spectrum at $\lambda = 650$ nm gave main features at 401 and 472 nm. These maxima coincide with absorption bands observed in dmf solution at 405 and 470 sh nm. On the other hand, no emission was observed in a dmf solution of **1**. Only when samples were excited between 320 and 360 nm, a weak emission could be detected at 440 nm. The corresponding excitation spectrum yielded an intense, relatively narrow band with a maximum at 340 nm, responsible for the emission activity.

Emission spectroscopy of dinuclear **2** (Figure 7) gave essentially the same results for the solid *and* the dmf solution at room temperature. Excitation at 490 nm resulted in broad unstructured emission bands with maxima at 700 nm for the solid or at 660 nm in dmf, respectively. Resonance Raman experiments yielded essentially similar emission results. The excitation spectrum of **2** in the solid ($\lambda = 720$ nm) showed maxima at 398, 439 sh, 470, and 502 nm that in dmf ($\lambda = 700$ nm) gave maxima at 405, 435 sh, 460, and 550 nm. These values are in good agreement with the absorption maxima found at 400 sh, 435, 465, and ca. 550 nm for the dmf solution of **2** with two d^8 metal centers. While dinuclear

Table 9. Selected Calculated Lowest TD-DFT Singlet Transition Energies and Oscillator Strengths for **1**

		G98/B3LYP (vacuum)		G98/B3LYP PCM (CH_2Cl_2)		
state	main character (in %)	trans. energy[a] (wavelength)[a]	osc str	trans. energy[a] (wavelength)[a]	osc str	expt (CH_2Cl_2): λ_{max}/ϵ[b]
$^1B_2$	98 ($6a_2 \rightarrow 9b_1$) (HOMO $\rightarrow$ LUMO)	2.00 (620)	0.002	2.56 (484)	0.002	470 sh
$^1A_1$	77 ($8b_1 \rightarrow 9b_1$); 19($6a_2 \rightarrow 7a_2$) (HOMO $-$ 2 $\rightarrow$ LUMO)	2.51 (494)	0.044	3.00 (412)	0.049	413/2200
$^1B_2$	96 ($6a_2 \rightarrow 10b_1$) (HOMO $\rightarrow$ LUMO + 1)	2.82 (439)	0.013	3.41 (363)	0.012	365 sh
$^1A_1$	54($6a_2 \rightarrow 7a_2$); 40 ($8b_1 \rightarrow 10b_1$) (HOMO $\rightarrow$ LUMO + 2)	3.06 (405)	0.004	3.06 (405)	0.004	390 sh
$^1A_1$	55 ($8b_1 \rightarrow 10b_1$); 24 ($6a_2 \rightarrow 7a_2$); 14 ($8b_1 \rightarrow 9b_1$) (HOMO $-$ 2 $\rightarrow$ LUMO + 1)	3.37 (367)	0.094	3.89 (318)	0.066	300/7200

[a] Transition energies in eV; wavelengths in nm. [b] Absorption maxima in nm; molar extinction coefficients in M^{-1} cm^{-1}.

Table 10. Selected Calculated Lowest TD-DFT Singlet Excitation Energies and Oscillator Strengths for 2

		G98/B3LYP (vacuum)		G98/B3LYP PCM (CH_2Cl_2)		
state	main character (in %)	trans. energy[a] (wavelength)[a]	osc str	trans. energy[a] (wavelength)[a]	osc str	expt (CH_2Cl_2): λ_{max}/ϵ[b]
$^1B_{2u}$	98 ($5b_{1g} \rightarrow 8b_{3u}$) (HOMO $\rightarrow$ LUMO)	1.69 (734)	0.002	2.06 (603)	0.001	550 br[c]
$^1B_{1u}$	84 ($6b_{2g} \rightarrow 8b_{3u}$), 14 ($5b_{1g} \rightarrow 5a_u$) (HOMO $-$ 4 $\rightarrow$ LUMO)	2.07 (598)	0.094	2.42 (513)	0.093	465/3300
$^1B_{2u}$	92 ($4a_u \rightarrow 7b_{2g}$) (HOMO $-$ 1 $\rightarrow$ LUMO + 1)	2.58 (480)	0.013	3.22 (385)	0.014	435/3200[d]
$^1B_{1u}$	74 ($5b_{1g} \rightarrow 5a_u$), 84 ($7_{3u} \rightarrow 7b_{2g}$) (HOMO $\rightarrow$ LUMO + 2)	2.75 (452)	0.021	3.10 (399)	0.009	

[a] Transition energies in eV; wavelengths in nm. [b] Absorption maxima in nm; molar extinction coefficients in M^{-1} cm^{-1}. [c] Weak absorption tails down to ca. 650 nm. [d] Alternatively, this band may be assigned as a vibronic sideband of the 465 nm band.

complexes of bpym with d^6 metal centers are typically poor emitters,[24,55] there are dicopper(I) (d^{10}) complexes with strong luminescence in the solid and in solution.[42]

Tables 9 and 10 summarize the TD-DFT G98/B3LYP-calculated transition energies of the lowest-lying electronic transitions together with their character for **1** and **2**. Calculations using ADF/BP gave the same transition characters but lower excitation energies and are not listed there. The calculated transition energies correspond to the gas-phase situation and are lower than those observed in solution, a result not unexpected for planar systems open to solvent influence. To estimate the shifts of transition energies due to solvation, the TD-DFT procedure is applied to Kohn−Sham orbitals calculated by the polarized continuum model (PCM).[41] As a consequence of the larger separation of frontier orbitals, the calculated transitions approximated within PCM(CH_2Cl_2) are shifted to higher energies, thus generally corresponding better to the experimental results. The calculated blue shift is in agreement with experimental trends within these complexes.

The lowest-energy transitions calculated for **1** correspond to the excitations from MOs formed mainly by Pt and Cl orbitals into the π^* of the bpym ligand. They can be characterized as mixed metal-to-ligand charge transfer (MLCT) transitions with some halide-to-ligand (XLCT) contributions. The lower-lying transitions within **2** have similar character. The lowest broad absorption band is assigned to the HOMO($5b_{1g}$) $\rightarrow$ LUMO($8b_{3u}$) transition. The more intense and slightly solvatochromic bands were attributed to the symmetry-allowed MLCT/XLCT transitions (mainly $d_{xz} \rightarrow \pi^*$).

On reduction to the radical anions, there are weak (forbidden) intraligand transitions expected in the near-infrared region.[7,15,23] While these could be detected for $\mathbf{1}^{\bullet-}$ (Figure 8, Table 4) by OTTLE spectroelectrochemistry,[26] the poorly soluble system $\mathbf{2}/\mathbf{2}^{\bullet-}$ did not allow a detection of such features. However, the typical intense band at about 450 nm for dinuclear complexes of $bpym^{\bullet-}$ [15,23] could be observed (Table 5).

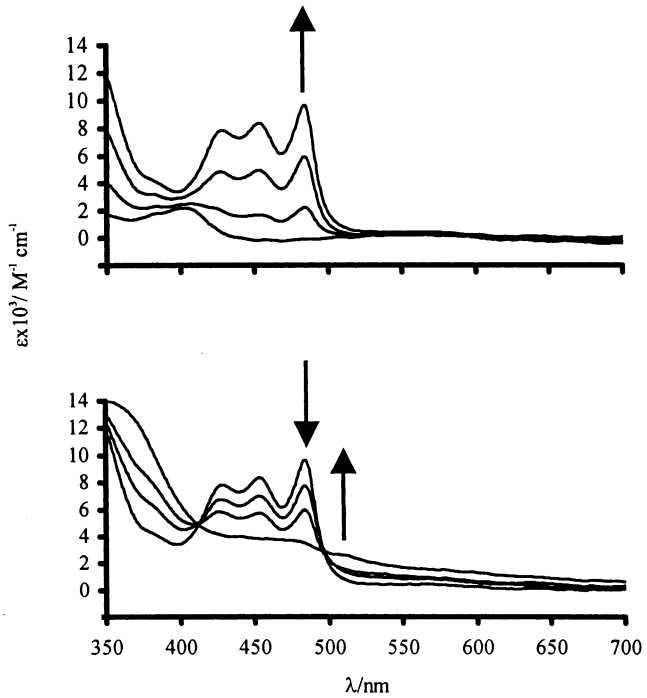

Figure 8. Spectroelectrochemical reduction of **1** to $\mathbf{1}^{\bullet-}$ (top) and of $\mathbf{1}^{\bullet-}$ to $\mathbf{1}^{2-}$ (bottom) in dmf/0.1 M Bu_4NPF_6.

The relatively small symmetrical complexes **1** and **2** are well suited for vibrational spectroscopy, including resonance Raman studies. We have previously reported corresponding results for other bpym-bridged compounds, viz., (μ-bpym)-$[M(CO)_4]_2$, M = Mo and W.[24]

Resonance Raman spectra could be obtained for **1** only on excitation at 488 or 458 nm. Both wavelengths lie within the low-intensity absorption bands of **1**. The rR spectra show rather weak resonances at 1565, 1497, 1225, 1018, 923, 878,

(55) (a) Hunziker, M.; Ludi, A. *J. Am. Chem. Soc.* **1977**, *99*, 7370. (b) Vogler, A.; Kisslinger, J. *Inorg. Chim. Acta* **1986**, 115, 193.

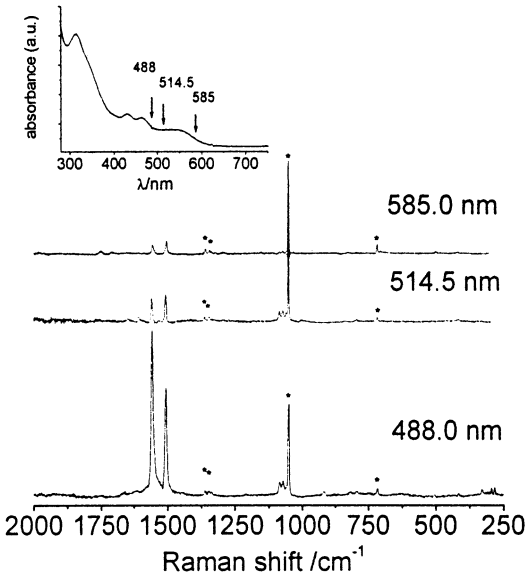

Figure 9. Resonance Raman spectra of **2** in KNO_3 at various wavelengths (absorption spectrum and excitation wavelengths in the insert; asterisks indicate NO_3^- vibrations).

673, 570, and 454 cm^{-1}. The first six of them are quite similar to resonances observed for the free ligand and the related tungsten complex (bpym)$W(CO)_4$;[24] DFT calculations yield values of 1596 and 1510 cm^{-1} for the highest Raman-active vibrations associated with the bpym ligand.

On irradiation at 597, 532, or 514.5 nm into the long-wavelength absorption band of dinuclear **2** the resonance Raman spectra also show weak resonances at 1560, 1509, 1085, 1071, 815, 793, 499, and 416 cm^{-1} (Figure 9). However, upon irradiation at 488 or 458 nm into the partly structured *second* absorption band the rR spectrum showed strong intensity enhancement of some of these bands, particularly those at 1560 and 1509 cm^{-1}. Further resonances are now observed at 1336, 1089, 1077, 924, 790, and 302 cm^{-1} whereas the bands at 499 and 417 cm^{-1} have disappeared. DFT calculations of Raman-active frequencies associated with the high-energy bpym stretching vibrations yield values of 1637 and 1520 cm^{-1}; the corresponding modes are illustrated in Figure 10.

The resonance Raman results can be discussed in connection with the assignments given above. As long as low-intensity MLCT bands are involved, no strong resonance enhancement is observed for both the mono- and dinuclear complex. Upon irradiation into the second band of the dinuclear complex a very strong enhancement of typical vibration modes of the bridging chelate ligand[24] is observed. In view of the findings for related dinuclear complexes (μ-bpym)$[M(CO)_4]_2$ (M = W or Mo)[24] the occurrence of at least two different MLCT transitions has to be considered. The absorption spectra of **1** and **2** are quite similar to those of the molybdenum(0) or tungsten(0) complexes as is the rR behavior upon excitation into the two distinguishable absorption bands. On the basis of the rR results for (μ-bpym)-$[M(CO)_4]_2$,[24] these two bands have been assigned to the HOMO−SLUMO as the lower and the SHOMO−LUMO as the higher, more intense transition. The resonances at 1557

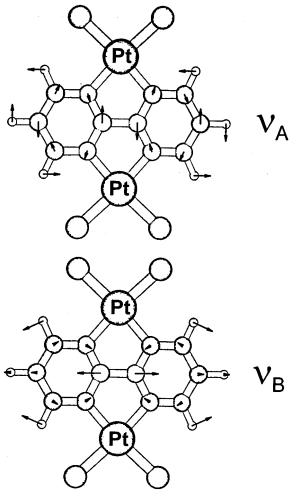

Figure 10. Pictorial representation of Raman active vibrations for **2** calculated at 1637 cm^{-1} (ν_A) and 1520 cm^{-1} (ν_B).

and 1478 cm^{-1} (for M = W) were found to change in relative intensity on going from band I to band II (the former increases), and in addition, a band at 1332 cm^{-1} emerges which was attributed to the inter-ring vibration ν(CC) and is consequently enhanced only when the LUMO is the target orbital. For the present dinuclear complex **2** we found exactly the same behavior. The 1560 cm^{-1} band of **2** gradually gains in intensity as compared to the 1506 cm^{-1} band when going through the excitation wavelengths from 597 to 514.5 nm. However the inter-ring vibration ν(CC) is much weaker than observed for the $M(CO)_4$ derivatives.[24] Similar behavior was observed for the two related complexes $(CO)_5MnRe(CO)_3$-(μ-bpym)$W(CO)_4$ and $(CO)_5MnRe(CO)_3$(μ-bpym)$Re(CO)_3Br$ where also a strong enhancement of ν(CC) was found for the former species whereas the latter compound showed a much weaker such resonance.[56] Only if there is already an appreciable amount of electron density at the ring-connecting C atoms in the π^* orbitals of bpym in the ground state, the effect on that C−C bond by the CT transition appears to be strong enough to give rise to a significant rR effect for this vibration. In agreement with the other results of this study the $[PtCl_2]$ complex fragment must then be considered a relatively weak π-donor toward such ligands.

Acknowledgment. This work was supported by the Deutsche Forschungsgemeinschaft, Fonds der Chemischen Industrie, and European Community (Program COST D14). Support of this work from the Ministry of Education of the Czech Republic and the DLR (Bonn) for KONTAKT Project CZE 00/013 is gratefully acknowledged. We thank Dr. Falk Lissner for X-ray data collection and the EPSRC (U.K.) for funding of the multifrequency EPR Centre at Manchester, U.K.

Supporting Information Available: Details of the X-ray structure determination in CIF format. This material is available free of charge via the Internet at http://pubs.acs.org.

IC020158F

(56) van Outersterp, J. W. M.; Stufkens, D. J.; Fraanje, J.; Goubitz, K.; Vlcek, A., Jr. *Inorg. Chem.* **1995**, *34*, 4756.